

Theoretical Implementation of Stochastic Epileptic Oscillator Using a Tripartite Synaptic Neuronal Network Model

JiaJia Li*, Peihua Feng, Liang Zhao, Junying Chen, Mengmeng Du, Yangyang Yu, Ying Wu*

¹ School of Information and Control Engineering, Xi'an University of Architecture and Technology, Shaanxi, Xi'an, 710055, China;

² State Key Laboratory for Strength and Vibration of Mechanical Structures, National Demonstration Center for Experimental Mechanics Education, School of Aerospace Engineering, Xi'an Jiaotong University, Xi'an 710049, China

³ College of Science, Shaanxi University of Science & Technology, Xi'an 710021, China

(Correspondence should be addressed to lijiajia_dynamics@xauat.edu.cn; wying36@xjtu.edu.cn)

Abstract:

Epilepsy is a neurological disorder, always coming with abnormal brain seizures activity of complex randomness and unpredictability, which have brought obstacles for the improvement of epileptic treatment. However, the mechanism of the epileptic randomness has not been unfolded. Inspired by the recent experimental finding that astrocyte G protein coupled receptor involves in the stochastic epileptic seizures, we proposed a cortical tripartite synaptic network of neurons and astrocytes with the G protein noise, which is capable to explain the stochastic process of epileptic seizures in the involvement of the G protein noise, a Gaussian distributed noise which explains the heterogeneity of the G protein types and the nonuniform environmental effect. Based on this model, we have discussed the dynamical stochastic induction process of the epileptic seizures statistically by performing totally 60 simulation trials. Our simulation results showed that the increase of the noise intensity could induce the epileptic seizures state coexisting with the increase of frequency and in vitro epileptic depolarization blocks. Meanwhile, there has been a bistable state of the noise intensity for the neurons switching among the regular sparse spiking and the epileptic seizure state. This random presence of epileptic seizure state would be absent when the noise intensity continues to increase, then the neurons start to stay in epileptic seizures steadily, but with an increase of the epileptic depolarization block duration. The simulation results also shed light on the fact that the calcium signals in astrocytes have played significant roles in the pattern formation of both the random and steady epileptic seizure state. Our results on the stochastic process of the epileptic seizures could provide potential theory for improvement for the epileptic prediction and treatment.

1. Introduction:

Epilepsy is a worldwide neurological disorder where seizures occur randomly and generally comes with periods of unusual behavior, sensations, and sometimes loss of awareness. According to the recent report in Lancet [1], there have been over 70 million people suffering from epilepsy worldwide. Tremendous studies have focused on the treatment of epilepsy by simultaneously controlling the epileptic seizures with deep brain stimulation [2] or the anti-epileptic drugs [3]. Nevertheless, there's still high percentage of epilepsy population that are ineffective to these epileptic treatment pathways only for the lack of comprehensive knowledge on the mechanisms of epilepsy generation, including the randomness during the seizures [4, 5]. Therefore, unveiling the potential mechanisms of the epileptic seizure randomness emerges to be critical for a better understanding of both the epileptic generation and terminations. In previous methodological studies, some experts investigated the underpinning dynamical characteristics based on the epileptic electroencephalogram (EEG) data. For instance, Baud based on the regular temporal structure of epileptic EEG dataset to conclude against the conception that seizures are

completely random events [6]. Karoly and his team then utilized the statistical method to have detected the significant Interictal spikes information among the random epileptic seizure EEGs [7]. Even though, these EEG-based methodological studies lack the capability to explain the underpinning of the epileptic randomness in the view of micro biological neuronal networks.

To unfold the dynamical mechanisms of brain activities in the view of biological neuronal network, modeling studies based on the Hodgkin-Huxley and the related mathematical frameworks have been extensively used in explaining epileptic mechanisms. For example, Burn and his colleagues constructed a complex neuronal network model with rich -hub network structures to have proved the significant role of network rich hubs in the generation of synchronous epileptic seizures [8]. Kramer utilized the mean-field neural models to have explained the critical bifurcation phenomena during the long-lasting epileptic seizures [9]. Lytton and his colleagues also developed a computer simulation frame to have successfully retrieve the dynamical transitions between epileptic tonic and clonic phases [10]. Besides, astrocytes that was disregarded for a long time have been found in recent decades to be critical for the epileptic seizures and their stochastic characteristics [11–15]. Recent studies have developed models to study the modulating dynamics of astrocytes in epileptic seizures in different fields. For example, Witthoft and his colleagues established the models of potassium disusing in gap- junction channels to propose that the astrocyte gap junction block contributes to the epileptic seizures due to the degradation of potassium buffering function [16]. Similarly, Ullah and other teams demonstrated that the astrocyte also buffer inositol triphosphate (IP3) and glucose, which contributes to the epileptic seizures [17, 18]. In the view of astrocyte glutamate modulation effect, Nadkarni and his colleagues have performed a bifurcation analysis of the CA3 neuron-astrocyte local systems and proved that the astrocyte glutamate playing significant roles in decreasing the epilepsy generation threshold [19, 20]. Additionally, our previous modeling study also proved the positive role of abnormality of the astrocyte glutamate degradation in epileptic generation [21], which was found in in vitro experiment [22].

Because of the high correlations between the astrocytes and neuronal functions, unveiling the randomness mechanism of the epileptic seizures could be directed to the astrocytes. As recent experiments reported, there were diverse types of G-protein such as G_q and $G_{i/o}$ types [23–25]. G-protein-coupled receptors impose much effect on the astrocytes calcium (Ca^{2+}) signals and also indirectly affects the feedback modulation of astrocytes onto the neurons, therefore, there are high potentials of astrocyte G-protein heterogeneity among the population modulating the stochastic dynamical activities of the neurons and astrocytes. This inspired us to propose that this diversity and heterogeneity of GTPase-Activating protein (G-protein) among the astrocyte population, G-protein noise, can partly explain the randomness of the epileptic seizures. In order to investigate the underlying mechanism of the G-protein noise modulating the stochastic epileptic seizures of neurons, we have developed a tripartite synaptic neuron-astrocyte network mathematical framework which incorporates and the G-protein noise in the astrocyte IP3 kinetic model.

By simulating the growing condition of the G-protein noise, we firstly discussed the state transitions of the epileptic seizure versus the increase of the noise intensity in 60 times of simulation trials. As well, we also studied the underlying mechanisms of the long- lasting dynamics of the noise-induced epileptic seizure by analyzing the correlation between neuronal firing dynamics in amplitude and frequency domains, the astrocyte long-lasting signals(the intracellular calcium signals in astrocytes), and the seizure durations enlargements in consequence of the increase of the noise intensity. Finally, the reasonability and the parameter values of our simulated results have been discussed with the related experiments and previous theoretical studies in the discussion section.

2. Models and Materials:

In the last two decades of years, the neural field model have been developed from the globally coupled miro- neural oscillation model [26] to describe macro EEG signals of the complex potential activities of brain normal cognitive [27–29] and disordered brain diseases including epilepsy [30–34]. The epileptic seizures in multiple-unit potential or the single EEG channel potential have been extensively studied by the mean-filed neuron model, However, because of its limitation for only describing the fast brain activities in milliseconds, it lacks the capacity to describe the long lasting and random dynamics of epileptic seizures in seconds, which could be redeemed by incorporating the slow system of astrocyte, therefore, our team has introduced the astrocytes into the model based on the basic principle of the neuron-astrocyte couple systems in micro scale. Finally, the network scheme termed TSNA (tripartite synaptic neuron-astrocyte) network have been established and depicted in Fig. 1.

As shown in the TSNA network in Fig. 1, on the biological basis of the neuron-astrocyte communication circuits in experiments[35, 36], we defined that the synaptic puffs of the glutamate from the other neurons in the network activate not only dendrites of the target neuron, but also the neighboring astrocytes, leading to an astrocytic Ca^{2+} -dependent feedback to the dendrites as well. Consequently, the target neuron receives not only direct synaptic puffs but also the transformed synaptic puffs from astrocytes, which makes a very high efficiency of synaptic information transmission observed in in vivo cortical studies [37, 38], therefore, it's more cogent to use the TSNA network model to investigate the epileptic seizure in contrast with seizures.

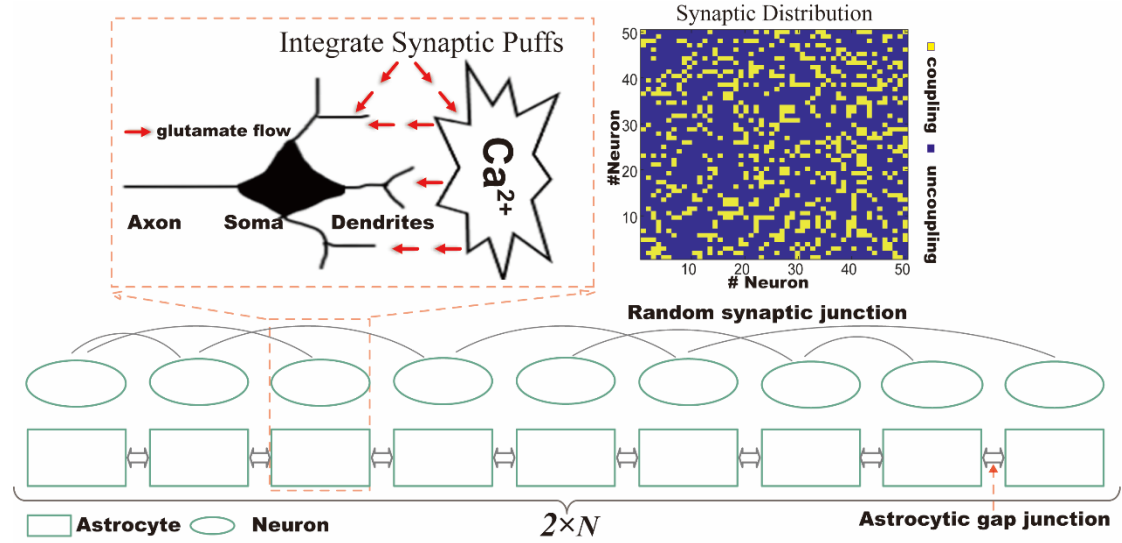


Fig. 1. Tripartite synaptic neuron-astrocyte network scheme. In the upper left panel inhibit the neuron-astrocyte circuit in local network, where the integrate synaptic puffs of the glutamate from the other neurons in the network activate not only the dendrite of the target neuron, but also the neighboring astrocytes, leading to an astrocytic Ca^{2+} -dependent feedback to the dendrites as well; At the bottom of the TSNA network, the model includes N pairs of neuron-astrocyte circuits. The neurons are coupled with the chemical synaptic connections and the astrocytes are coupled by the nonlinear gap junction channels. The top right panel of the connection map represents the connection state across all neurons. The synaptic connection probability was chosen as 0.18 that is close to brain cortex parameter domain.

In the TSNA network, for describing the correlation between the astrocytes and neurons more reasonable, we have utilized the biophysical Li-Rinzel model [39] to simulate the Ca^{2+} activity in each astrocyte:

$$\frac{d[Ca^{2+}]_i}{dt} = c_1 v_1 p_\infty^3 n_\infty^3 q^3 ([Ca^{2+}]_{ER} - [Ca^{2+}]_i) + c_1 v_2 ([Ca^{2+}]_{ER} - [Ca^{2+}]_i) - \frac{v_3 [Ca^{2+}]_i^2}{[Ca^{2+}]_i^2 + k_3^2} - J_{leak} \quad (1)$$

$$\frac{dq_i}{dt} = \alpha_q(1 - q_i) + \beta_q q_i + \xi_i(t), \quad (2)$$

$$p_\infty = \frac{[\text{IP}_3]_i}{[\text{IP}_3]_i + d_1}, n_\infty = \frac{[\text{Ca}^{2+}]_i}{[\text{Ca}^{2+}]_i + d_5}; \quad (3)$$

$$\alpha_q = a_2 d_2 \frac{[\text{IP}_3]_i + d_1}{[\text{IP}_3]_i + d_3}, \beta_q = a_2 [\text{Ca}^{2+}]_i. \quad (4)$$

In the Li-Rinzel model, the membrane leaky current J_{leak} was introduced [20] to represent the Ca^{2+} ions balance between inter- and extra-cellular astrocyte endoplasmic reticulum (ER). It has the mathematical form of $k_{leak}([\text{Ca}^{2+}]_i)$. $\xi_i(t)$ represents the zero mean, uncorrelated, and Gaussian white noise sources with $\langle \xi_i(t) \xi_i(t') \rangle = 2\alpha_q \beta_q / (a_q + \beta_q) / N$, where N is proportional to the number of ion channels in the ER membrane. Obviously, the channel noise intensity is proportional to $1/N$.

The glutamate-binding receptors locating on the surface of the astrocyte membrane listens to neuronal abundant firing activities in response to abrupt increase of IP3 and Ca^{2+} in cytoplasm sequentially. This process was modeled by Nadkarni et al. [20] with a dynamical equation to describe the proportional relation between the IP3 increase rate and released concentration of the neurotransmitter. However, in order to consider the heterogeneity among those G-protein coupled receptors among the astrocyte populations in a comprehensive view, we have introduced the noise into the model [20], then the final IP3 model has the following form:

$$\frac{d[\text{IP}_3]_i}{dt} = \frac{([\text{IP}_3]^* - [\text{IP}_3]_i)}{\tau_{ip3}} + r_{ip3} \frac{(\rho_{glu} [\text{glu}]_{neuron})^n}{(\rho_{glu} [\text{glu}]_{neuron})^n + k^n} + DS \xi_i(t) + J_{astro-gap}^i. \quad (5)$$

On the right of IP3 dynamical model, the first term represents the decaying process of intracellular IP3 due to enzymes, with the degradation time constant of τ_{ip3} and equilibrium concentration of $[\text{IP}_3]^*$, the second formula explains the increases of IP3 concentration modulated by the glutamate binding the G-protein receptors, with the binding intensity of r_{ip3} , and the glutamate binding the G-protein receptor follows the Hill formula to describe the saturation characteristics of G-protein binding rate due to the increase of glutamate concentration. ρ_{glu} is the vesicle to extra-synaptic volume fraction of the integrate synaptic glutamate puffs in Fig. 1. The glutamate puff from each neuron follow the law:

$$J_{astro-gap}^i = [\text{T}]_i(V_{s,i}) = 1 / (1 + \exp(-(V_{s,i} - V_T) / \kappa)), \quad (6)$$

and the integrate synaptic glutamate puffs $[\text{glu}]_{neuron}$ is the sum of the glutamate from the neurons located 1.5 radius center-to the current astrocyte. In the IP3 dynamical model, the glutamate represents the collective glutamate puff from all other neurons in the network, finally obtaining a summation form of $\gamma \sum_{i=1}^N [\text{T}]_i(V_{s,i})$, where γ represents the ratio of those glutamate that successfully target to the postsynaptic receptors in the dendrites. The mathematical form of $[\text{T}]_i$ can refer to Eq. (6), and the parameter values in the equation were selected from Destexhe et al. [41].

For simplicity, the biding noise of neuronal glutamate onto the G-protein receptors, the G-protein noise, was defined as Gaussian white noise with intensity of DS to describe the heterogeneity between different astrocytes in a limited tissue of network. The noise involves a standard distribution with the mean $\langle \xi(t) \rangle = 0$, and the noise correlations are described by $\langle \xi(t) \xi(t') \rangle = \delta(t - t')$.

In the astrocyte network, the gap-junctional connections among the astrocytes are described by the nonlinear gap-junction model proposed by Goldberg et al. [40] to describe threshold and nonlinearity of the IP3 flow motivated by the pulse-shaped Ca^{2+} activities in astrocytes:

$$J_{astro-gap}^i = g_{astro-gap} \sum_{j=i-1, i+1} -(1 + \tanh(|IP3_i - IP3_j| - 0.3) / 0.05) \quad (7)$$

For studying the epileptic seizure of the TSNA network which includes both the soma and dendrites, we have utilized the two-compartment pyramidal models including the dynamical membrane potentials of both soma (V_s) and dendrite (V_d) [42], and see the Appendix for the detailed biophysical models of this Rinsky-Rinzel model. Wherein, the two membrane potentials obtain their updated forms in the TSNA network as shown in following equations:

$$C_m \frac{dV_{s,i}}{dt} = I_{Leak}^s(V_{s,i}) - I_{Na}^s(V_{s,i}, n_i) - I_{K-DR}(V_{s,i}, n_i) + \frac{g_c}{p}(V_{d,i} - V_{s,i}) + \frac{I_{astro,i}}{p} \quad (8)$$

$$C_m \frac{dV_{d,i}}{dt} = I_{Leak}^d(V_{d,i}) - I_{Ca_{neuron}}(V_{d,i}, s_i) - I_{K-AHP}(V_{d,i}, w_i) - I_{K-C}(V_{d,i}, c_i) + \frac{g_c}{1-p}(V_{s,i} - V_{d,i}) + \frac{I_{astro,i}}{1-p} + I_{syn,i} \quad (9)$$

In the network model scheme, each neuronal soma receives the input current from the coupled dendrite ($g_c/p \times (V_{d,i} - V_{s,i})$) and the feedback current of the neighboring astrocyte ($I_{astro,i}/p$). Each ensemble dendrite receives feedback effects from the integrate synaptic current of the other network neurons ($I_{syn,i}$) and the feedback current of the neighboring astrocyte ($I_{astro,i}/(1-p)$). Those transmembrane ion channel currents of in the soma and the dendrite can be described as the function of the corresponding potentials ($V_{s,i}$ and $V_{d,i}$) and the ion channel opening variables, whose mathematical equations are shown in the Method section of the Appendix.

Meanwhile, in the model scheme, the integrates synaptic inputs from other neurons in a homogeneous all-to-all random connection (HAAR). The homogeneity is chosen for the consideration of the weak distance-dependent effects in a small network scale of less than thousands of neurons. The homogeneous all-to-all random connection can be described by the integrate synaptic current:

$$I_{syn,i} = g_{syn} \left(\sum_{i=1}^N W_i s_i \right) (V_{s,i} - E_{syn}), \quad (10)$$

where the synaptic weight $W_j = 1$ with the connection probability of 0.18, and $W_j = 0$ with the probability of 0.82. The connections probability was defined as 0.18 that is close to brain cortex parameter domain [43]. The connection map between neurons in one representative simulation trial was depicted in the upper right panel in Fig. 1.

The fraction of open channels s can be obtained by the dynamical equation of

$$\frac{ds}{dt} = \alpha_s \cdot \text{heaviside}(V_s - 20) - \beta_s \cdot s, \quad (11)$$

where the parameter values of the rise rate α_s and decay rate β_s of the fraction s can be found in Table 1 in the Appendix.

In this paper, we developed the potassium reversal potential V_K as a variable instead of constant value based on the method of Fröhlich [44]. The kinetic dynamical equations are described by the Nernst equations and involve the mathematical forms of

$$V_K = -26.64 \log((K_{out} / K_{in})) \quad (12)$$

Here the K_{in} was defined as a constant value of 130mV for both soma and dendrite, and the K_{out} represent the accumulation of both soma and dendrite potassium channel efflux, and had the dynamical equation:

$$\tau_K \frac{dK_{out}}{dt} = \kappa_K I_{K_{efflux}} - (J_{lateral-diffusion} + J_{bath-diffusion}) - J_{pump} - J_{astro} \quad (13)$$

In the above equation left, τ_K represents the biophysical time constant of the potassium concentration in the extracellular space.

The first term in Equation right present the total potassium efflux from the soma and dendrite, and involves the mathematical forms of $(I_{K-DR} + I_{K-C} + I_{K-AHP})$, the multiplication parameter $\kappa_K = zFV_{ast}$ denotes the physical scaling constant between the current and the potassium ion flux[45].

The J_{pump} arises from a backwards influx from extracellular space (ECS) and negatively contribute to the K_{out} . It has the mathematical form of $35/(1.0+(3.5/K_{out}))^2$ [44]; Meanwhile, the astrocyte in the local circuit environment still intake potassium by Kir4.1 and water channels, and this process of J_{astro} was modeled as $g_{astro_max}/(1.0+\exp((18.0-K_{out})/2.5))$ [44].

After all, the local potassium ion can diffuse in two ways: between different local circuits, and between the local cell circuit and the base potassium environment outside the current network of neuron and astrocyte cell environment, therefore the intercellular lateral diffusion flux $J_{lateral-diffusion}$ and the base-environment dependent potassium flux $J_{base-diffusion}$ have been added into the K_{out} dynamical model [17], and they obtained the mathematical forms of $\varepsilon_K (K_{out}(i-1) - 2K_{out}(i) + K_{out}(i+1))$ and $\varepsilon_K (K_{out} - K_{bath})$ respectively;

The biophysical definitions and values of all the parameters in above equations are listed in Table 1.

3. Results:

After the pre-synaptic released glutamate partially diffuse to the astrocyte that enwraps the post synapse, the astrocyte responds to neuronal activations through an increases of the second messenger IP3, but in the scale of neuronal networks, each astrocyte reacts differently even under the same neuronal stimulation due to the heterogeneity of the astrocyte G-protein receptors, the extracellular circumstances etc. Here in this paper, we utilize the noise intensity DS to represents the IP3 -reaction difference, detailed in the equations of the astrocyte IP3 dynamical models. The dynamical models in section 2 were simulated under $DS=0, 0.25, 0.5, 0.75, 1.0, 1.25, 1.5, 1.75, 2.0$ respectively, during which we recorded the all the variables of neurons and astrocytes. The representative simulation trial of the actions potentials neuronal network is depicted in Fig. 2. It clearly presents evolutions of the spatiotemporal patterns of the neuronal network when DS increases.

At the first glance in Fig. 2, when DS is equal to 0~0.75, all the neurons fire as a mixture of bursting and single spiking synchrony in the network. The bursting parts of firing tend to entail higher amplitude but randomly show up in the network, as can be seen in the spiking pattern map when DS is equal to 0~0.75. Because in the resting state of human brain, the firing of neuronal networks always in alpha oscillation with random gamma oscillations to keep the brain in highly self-organized, preparing for the coming events [46]. The neuronal network when DS is equal to 0~0.75 proximately reflects the focal firing pattern of resting state. When DS jumps into the range 1~2, the neurons start to fire as seizure-like pattern, a dynamical switching between spiking and depolarization block (DB). depolarization block is a typical seizure property with glutamate-induced long-lasting depolarization phase and high rate energy consumption. Here those glutamate inducing DB are compromised with astrocytic gliotransmitter and neurotransmitters. Meanwhile, the synchrony spatiotemporal pattern of the neuronal network arises from the randomly all-to-all synaptic distribution, shown in Fig. 1.

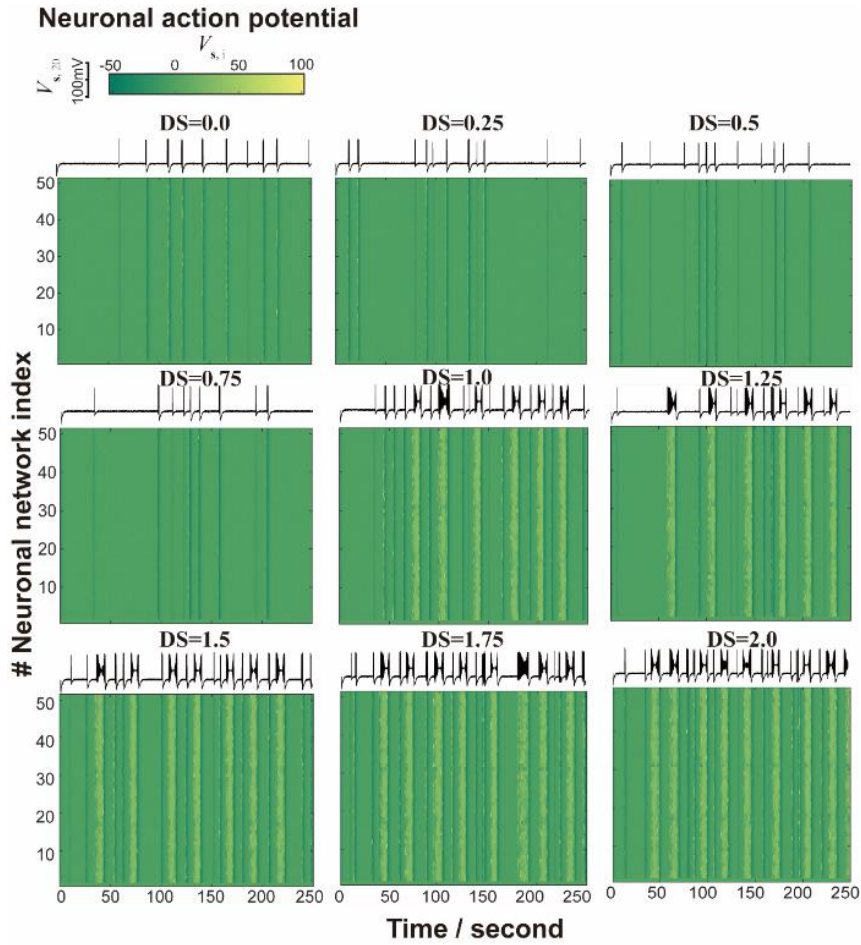


Fig. 2. Spatiotemporal firing patterns of the neuronal network exposure to the astrocyte G-protein noise. The 9 subfigures in this figure correspond to the case of noise intensity DS is equal to 0, 0.25, 0.5, 0.75, 1.0, 1.25, 1.5, 1.75, 2.0 respectively, the single neuronal firing in each subfigure is isolated from the 20th neuron in the network.

Meanwhile, 8 simulation trials of the single neuron firing patterns were presented when $DS=0.25$, 0.75, and 1.25 in Fig. 3 to discuss the randomness presence of epileptic seizures induced by the increase of the G-protein noise. In Fig. 3 the red rectangles represent the epileptic depolarization blocks. As has been presented in Fig. 3 initially, in each case of DS , the neuron firing pattern always emerges differently across simulation trials but obtains a different distribution under different DS . When $DS=0.25$, the neuron firing generally stays in a sparse spiking pattern. This sparse firing pattern could correspond to the brain state of resting state without the external stimulation. Furthermore, when $DS=0.75$, the presence probability of the epileptic seizures with depolarization blocks increase with the coexistence between the sparse firing and epileptic seizure patterns. This could correspond to the brain state of the bi-stability when the DS start to affect the brain initially. Finally, when DS increase big enough to 1.25, the neuron firing persistently keep in epileptic seizure state. This reflects that under this stat of G-protein noise, the brain has stayed in the epileptic state steadily.

All in all, Fig. 2 and Fig. 3 have depicted a clearly trends for the neurons transiting from sparse spiking to epileptic- seizure events in three phases: a stable sparse spiking pattern, a bi-stable coexistence of sparse- spiking and epileptic- seizure patterns, and the stable epileptic-seizure pattern, under the increase of astrocyte G-protein noise.

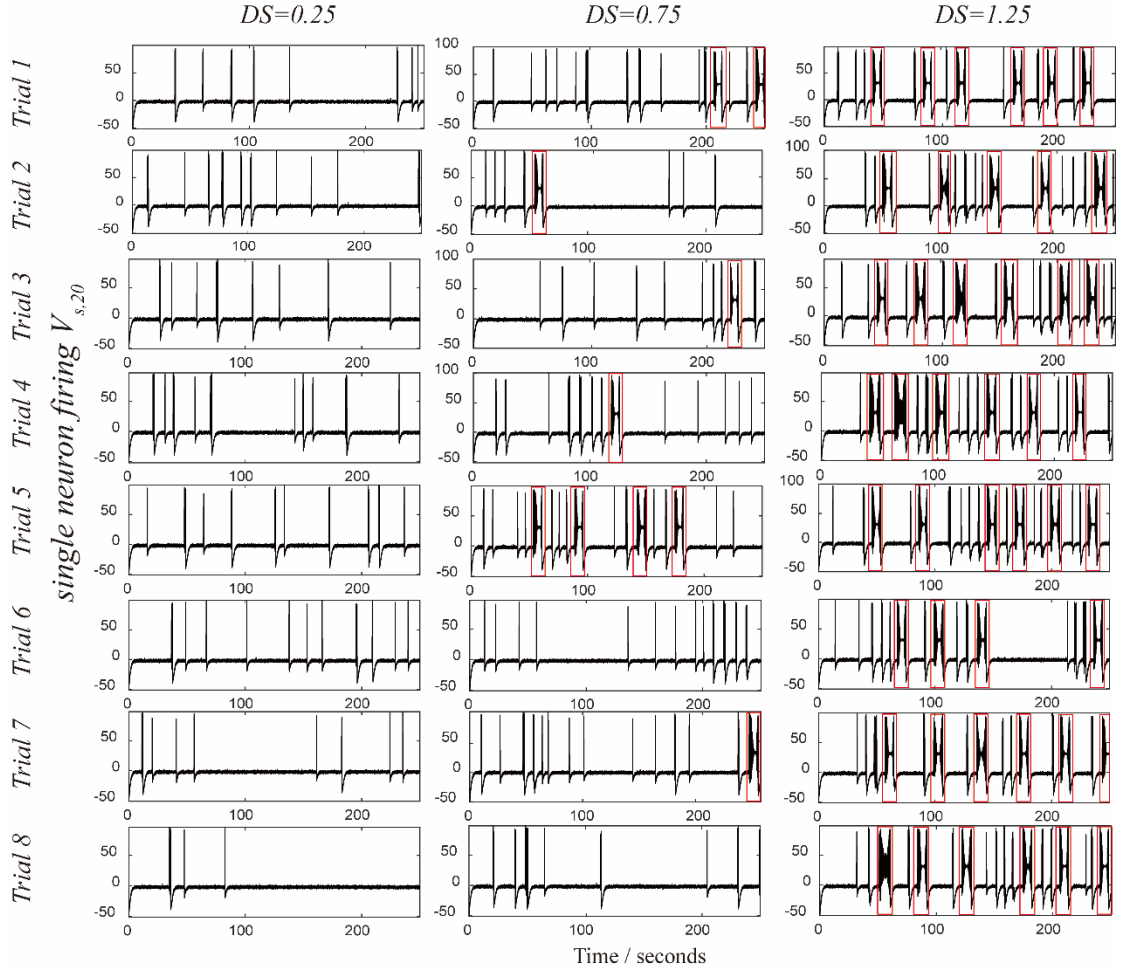


Fig. 3. The random presence of epileptic seizure with depolarization blocks at different G-protein noise intensity DS across different simulation trials. The total simulation trials for all cases of DS is 60, and only randomly 8 trials of single neuronal firing $V_{s,20}$ for each $DS=0.25, 0.75,$ and 1.25 are present for comparison. All the epileptic specific depolarization block phases during seizures are circled with red rectangles.

To accommodate the seizures results above, we have analyzed the collective firing pattern of neuronal network in comparison with the experimental mean-field potentials of epileptic seizures [47]. Therefore, the mean voltage and the integrate synaptic current, together with the single neuronal firing and the astrocyte Ca^{2+} and K^+ dynamics have been presented in Fig. 4. Because the dendrite branches are simplified into one dendritic model, therefore the sum of the currents I_{syn} represents the ensemble integrate mean field potentials of the focal neuronal network, namely being capable to study the mean-field potential characteristics. Meanwhile, the mean values of a focal neuronal network firing obtain the same capability for describing the neuronal mean-field potentials in a focal neuronal network. As shown in Fig. 4, the time series of single neuron(20th) firing, the ensemble synaptic current, and the mean voltages in contrast with the *in vitro* seizure in single neuron and extracellular mean field in the Fig. 3 of the ref. [47]. First, it's manifested in Fig. 4 that our simulated seizure in single neuron is composed with sparse spiking and the epileptic depolarization blocks that generally persist in a stable value for a short time, which is close to the *in vitro* seizure firing of single neurons [47]. Besides, in the collective view of the neuronal network dynamics, the simulated mean voltages closely resemble the time series of the ensemble synaptic current in Fig. 4, and they both involves a potential peak at the time towards the single neuronal depolarization block phase. Surprisingly, this correspondence between single neuron and mean

filed can also be found in the Fig. 3 (A) and (B) of ref. [47] *in vitro* seizures. On one hand, this vigorously shows the representative capacity of the synaptic current and the mean voltages for focal mean-field potential, on the other hand, the consistent presence of the correspondence between single neuron and mean filed in both the simulation and *in vitro* results indicates that the results in this paper is provable.

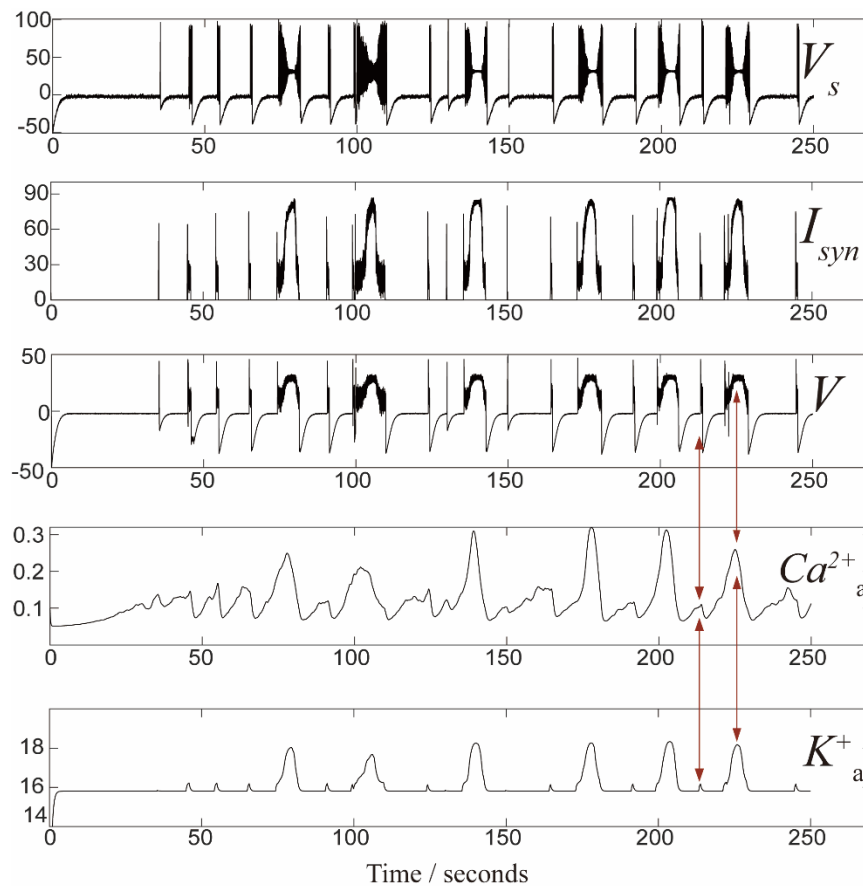


Fig. 4. The assembly synaptic current and mean voltage corresponding to the noise-induced seizure potential, together with the astrocyte oscillation pattern Ca^{2+} and K^+ dynamics during the epileptic seizure condition with $DS=1.0$.

Furthermore, the intracellular astrocytic Ca^{2+} and extracellular K^+ were dynamically studied in contrast with the epileptic seizure potentials. The results are placed in Fig. 4 bottom. Firstly, it's very easy to find out that the depolarization block phase in the seizure potentials parallels to the peaks of Ca^{2+} and K^+ , which reflects the experimental results of that the depolarization-block seizure firing induces much more glutamate released onto astrocytes and excite astrocytes with much higher IP3 and Ca^{2+} concentrations sequentially. Meanwhile, the depolarization block phase of seizure potentials give rise to the inwardly Na^+ channels but inhibits the outwardly K^+ channels. This directly renders the extracellular spaces with a much higher K^+ concentration. In the sight of the above modulations of astrocyte Ca^{2+} and K^+ in neuronal firing, the astrocyte has been a very sensitive partner to sense and response to neuronal seizure potentials in its Ca^{2+} and K^+ .

Seizure involves dynamical specificities not only in amplitude, such as results in Fig. 4, but also firing frequency. Therefore, we have studied the ensemble spectral power distribution during the frequency domain 0~500Hz and the time - frequency analysis based on the N neuronal potentials at the cases when the noise intensity $DS=0$ and $DS=1.0$ respectively. The simulation results are presented in Fig. 5. Firstly, in order to detect the high -frequency oscillation characteristics that are generally distributed among 80~500Hz [48], the frequency band of 0~ 500Hz was introduced to analyze the down-sampled-1000Hz

neuronal voltages data by Fourier transformation method. Fig. 5 (A) firstly exhibits the spectral power distributional difference across frequencies when $DS=0$ and $DS=1.0$ respectively. We can easily find out that the voltages data with IP3 noise interpretation exhibited much higher spectral power than no-noise case over the frequency range of about 80~400Hz. This gives a first glance of seizure events induced by the G-protein noise that involves the epileptic experimental High Frequency Oscillation, HFO characteristics. Moreover, the dynamical evolutions of the voltage frequency spectral power were studied to investigate the original components of those HFO in Fig. 5 (A). Firstly, it can be seen from Fig. 5 (B) upper that as $DS=1.0$, there were concentrated high frequency timings besides the moments when the seizure depolarization block happens. However, as $DS=0$, these concentrated high-frequency timings were not present during the entire time range. This comparably implies that the seizure depolarization can be a ‘‘HFO attractor’’ that finally induces the specific HFO phenomena in the epileptic seizures.

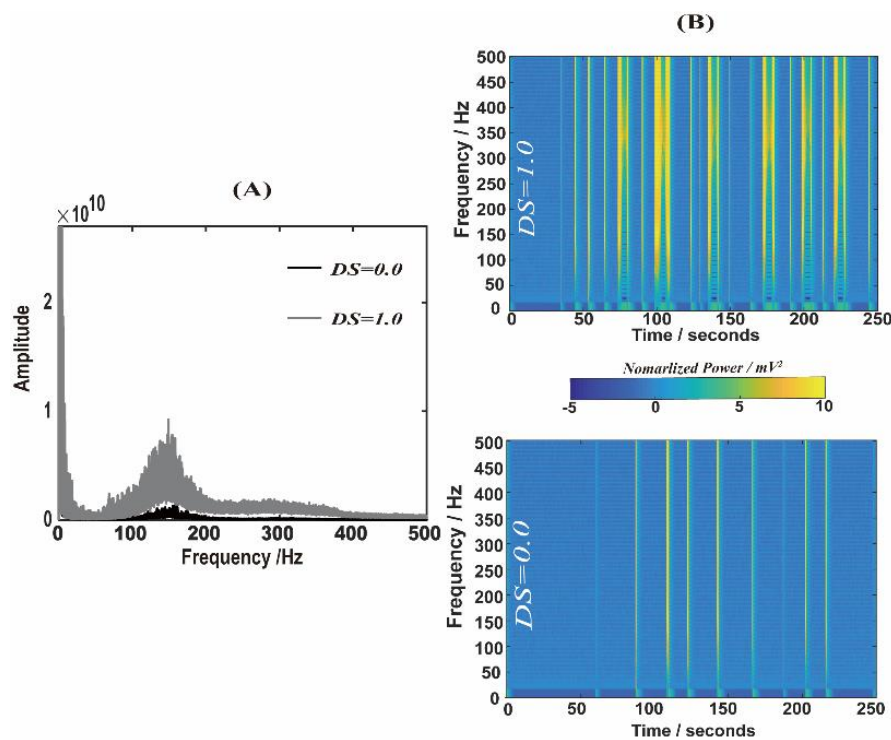


Fig. 5. Noise-induced neuronal frequency switches of the neuronal network. (A) the spectral power of the neuronal network firing averaged across different neurons when $DS=0.0$ and 1.0 ; (B) the normalized frequency versus time map when $DS=0.0$ and 1.0 respectively. The normalized power values were obtained using Fast-Fourier transform with non-overlapped window $0.125s$ (the total time is $250s$), and then were averaged cross neurons and normalized versus the baseline data from $0s\sim 10s$.

Generally, the epileptic seizure occurs randomly, however, it has been recently demonstrated that the epileptic patients convey bis-stable states of both regular and epileptic seizures, and the external stimulation could induce the transition between the two states [44]. Therefore, the epileptic seizure confers the characteristics of dynamical stability, which corresponds to the epileptic depolarization block in this paper. In order to measure the stable regulations of the epileptic DBs and find out the critical state of the epileptic seizure in the stochastic process, we introduced the seizure DB information entropy, the formula of the entropy computation method was placed in the supplementary material Method section, to statistically represent the seizure induction state, and utilize the t-test among 60 simulations trials in the DS condition to find out the significance for each case of DS compared with the control case $DS=0$. The entropy theory was generally used to describe the probability distributions of the spiking patterns

(words) in a series of simulated or experimental potentials[49–52], and it's more efficient to distinguish the ignorable changes of neural activities by analyzing the neuronal information entropy theory than the neuronal firing information directly[53]. In this paper, the intended “words” are the DBs, and the entropy of this potential series represents the seizure inducing degree in one case of G-protein noise. Meanwhile, the final DB entropy was obtained by averaging all entropy values across all neuron cells. The simulation results of the DB entropy versus the G-protein noise was depicted in Fig. 6. At the first glance, we can find out that the DB entropy gradually increases when $DS \geq 0.75$ and finally went into stable at about $DS = 1.25$. It implies that when the DS increases initially, the epileptic seizure events just start to induce but stay in a state with less numbers of DB presences, but when the noise intensity gradually grows, the epileptic seizure events induce more frequently with much more DB presence. Meanwhile, the statistical analysis provides us the information that the epileptic seizure events induce significantly in statistics when $DS \geq 0.75$. However, we can also find that there is epileptic seizure event absent in some case of simulation trial when $DS = 0.75$, this exactly predicts this state of criticality for the epileptic system of neurons and astrocytes. The DB presence at each DS value can be obtained based on the DB spatiotemporal patterns in Fig. 6.

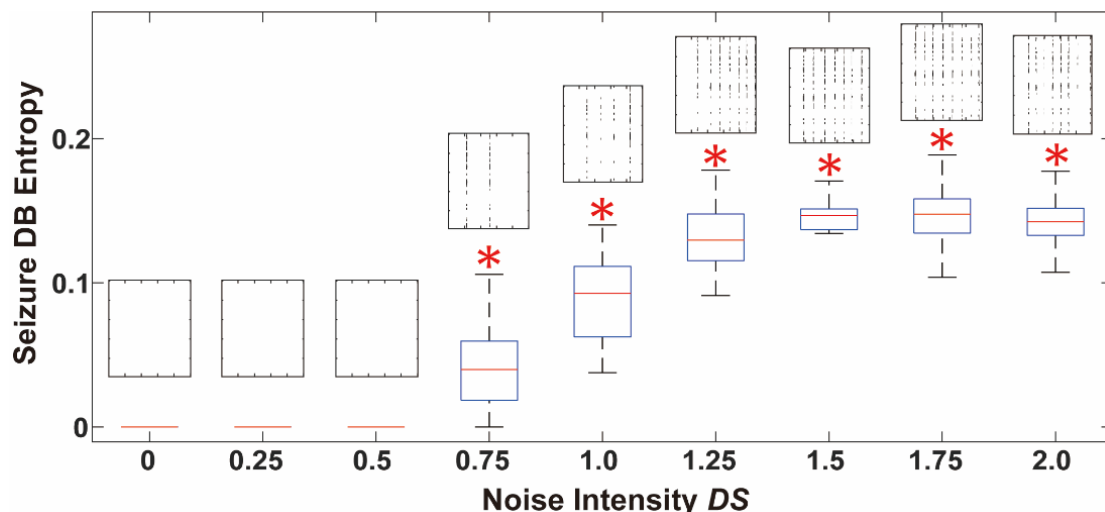


Fig. 6. The seizure DB map and entropy versus the noise intensity DS . The seizure DB map is obtained by filtering other voltage signal by defining a “1” for a sliding 1s if the difference between the maximal and minimal voltage values from this time window, and “0” for other cases. The DB entropy is obtained based on the DB map data by using the information equation in the Appendix Method section. Because of the randomness of seizure induction, 20 trials for each case of DS were performed and T-test is applied to all trials of $DS = 0.25, 0.5, 0.75, 1.0, 1.25, 1.5, 1.75, 2.0$ versus the control case $DS = 0$ with Bonferroni correction $\alpha = 0.025/8$. The “*” represents the DB entropy of one DS case versus the control is statistically significant.

Furthermore, for a biological investigation of the stochastic process of epileptic seizure under G-protein noise, we have measured the DB durations at different noise intensity cases. The DB duration statistics in Fig. 7 were done by averaging the all the DBs across all the neuron cells and depict the mean value and each point of the DBs of all simulation trials at each G-protein noise condition. All the DBs computed in seconds were in consistent with the related experiments of seizure duration measurements [54]. We can see from Fig. 7 that the DB duration stays in zero steadily as the $DS < 0.75$, however, when DS increases continuously, the DB duration elevated into a table value of about 18 seconds which is very close to the epileptic durations in experiments[54]. Therefore, the above Fig. 6 has

unfolded the formation process of stable epileptic seizure state in the sight of the Shannon entropy method, but Fig. 7 has statistically answered how degree the stable epileptic seizure becomes in the sight DB durations. Besides, this can partly indicate that our simulation method is trustful to unfold the stochastic process of epileptic seizure induction process.

As was demonstrated in earlier experimental studies, astrocytes can respond to epileptic seizures or the external cognitive tasks with long-lasting Ca^{2+} signals in intracellular astrocytes [55–61]. However, there remains some confusions on the dynamical characteristics after certain conditional stimuli when scientists found much abundant dynamical patterns of Ca^{2+} signals in astrocyte [62, 63]. Hereinto, we have manifested the unpinning of two-state astrocyte Ca^{2+} signal that underlines the complexity of the epileptic seizures. Therefore, we have studied the Ca^{2+} signal decoding in frequency and amplitude under the condition of the G-protein noise (IP3 non-block) versus the control condition (IP3 -/-) in order to compare the simulation results with experimental ones[61]. The frequency coding was extracted by doing the Fourier transformation for the simulation data of all trials and take the mean of the frequency power in Fig. 8 (A), and then depicting the mean and standard deviation of the maximal frequency of each simulation trial together with the re-drawn experimental data[61] in Fig. 8 (B). The spatiotemporal patterns of the Ca^{2+} signals in the case of both IP3-/- and IP3 non-block and the phase map of astrocytic Ca^{2+} systems were depicted in Fig.8 (C) and (D) to explain the multiple-amplitude-state phenomena of Ca^{2+} signals under epileptic seizures.

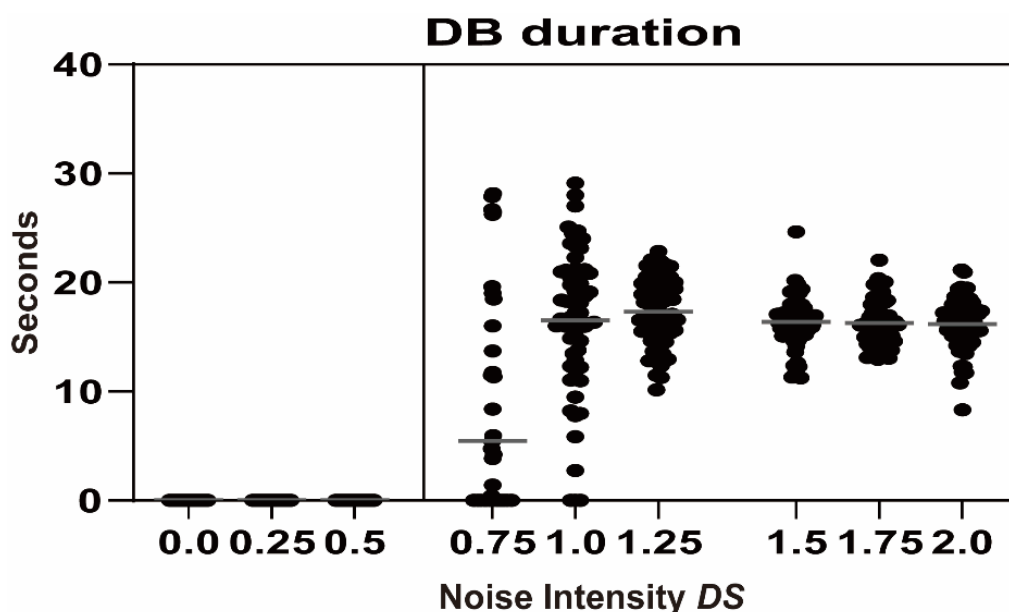


Fig. 7. Noise-induced seizure DB duration bifurcation versus the noise intensity. DB duration of all 60 trials of each DS is depicted in the figure, and each DB duration value in the figure was obtained by computing the interval between two DB starts and then do the average across the neuron cells.

Firstly, it can be seen from Fig. 8 (A) that the frequency of the Ca^{2+} signals tend to concentrate to about 0.05Hz when the G-protein- bounded receptor is not blocked(IP3 non-block), but to about 0.01Hz when the IP3 receptor is blocked. When we counted the mean and standard deviations of the peak frequency of Fig. 8 (A) and presented them in unit of /min, in contrast with the corresponding case of IP3-/- and IP3 non-block based on the experimental data [61]. From Fig. 8 (B), we can find out that under the IP3 non-block case, the mean and standard deviation of experimental and simulation data are both very close,

this indirectly imply that our established models in this paper are very helpful and reproducible to study the activities of epileptic seizure and astrocytes in vivo. However, there are still a small gap of about 1Hz between experimental and simulation case when IP3 is blocked (IP3^{-/-}). This mismatched gap could arise from other pathways of non-IP3-pathway induced Ca²⁺ signals, such as voltage-gated calcium channels (VGCCs) [45, 64] and store-operated calcium entry [65] etc. in vivo.

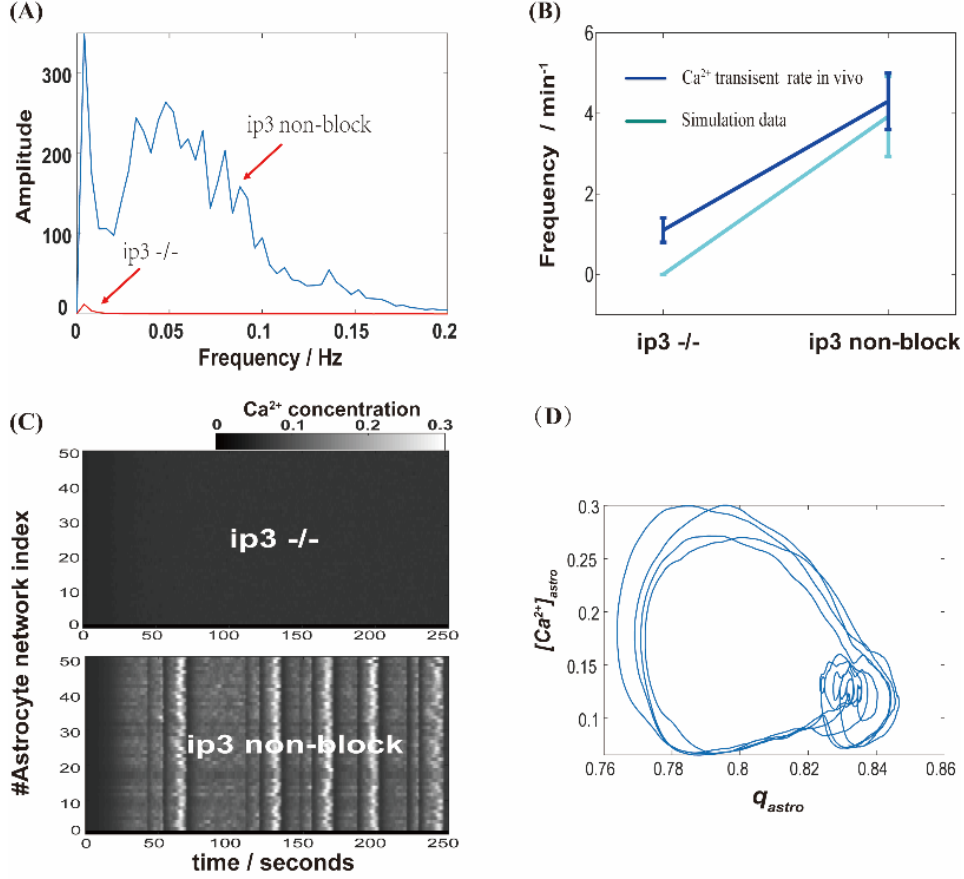


Fig. 8. Ca²⁺ transient kinetics of the astrocyte network due to G-protein noise versus in vivo. (A) The simulation results of the spectral power of Ca²⁺ transients in the astrocyte network when $r_{ip3}=0$ (ip3^{-/-}) and $r_{ip3}=0.28$ (ip3 non-block); (B) the mean rate of Ca²⁺ transients in the astrocyte network when IP3 stays in blocked and non-blocked in the conditions of in vivo versus simulation results respectively; (C) the population patterns of the Ca²⁺ transients in the astrocyte network when $r_{ip3}=0$ (ip3^{-/-}) and $r_{ip3}=0.28$ (ip3 non-block); (D) the phase map of astrocyte Ca²⁺ signal and the gating variable q_{astro} when $r_{ip3}=0.28$ (ip3 non-block).

4. Conclusion and Discussion:

Randomness of epileptic seizures has been the significant obstacle for the prediction and treatment of epilepsy. For investigating the stochastic process of the seizure generation, we have constructed the tripartite synapse network models of neurons and astrocytes that exhibit the G-protein noise. Our simulation results have shown that the dynamics of the epileptic seizures start to emerge in statistics when the G-protein noise intensity DS increases over a critical state. Surprisingly, at the critical value of DS , the neurons obtain the concomitant patterns of both sparse firing and the epileptic seizures. The above results can explain the common epileptic clinical cases, where the sever abnormality of brain damage after seizures always comes with higher rate of epileptic seizures for certain subjects [66]. Besides, the positive role of astrocytes in the epileptic seizure have also been shown in the paper. We proved that astrocytic Ca²⁺ signals tend to be activated after the increase of DS , accompanying with K⁺

concentration peaking. Additionally, Ca^{2+} and K^+ both can sustain the generation of depolarization block in single neuron and the abrupt mean field pulse at the time when Ca^{2+} and K^+ peak. In order to investigate the duration changes of the epileptic seizure under the G-protein noise and verify the reliability of epileptic seizure phenomena shown in this paper, the statistical DB duration among all simulation trials were studied versus the noise intensity DS , in contrast with the duration measurements in experiment[54]. Results have shown that the bigger DS is, the wider the DB durations will be, implying a severer epileptic seizure state. In the sight of Ca^{2+} signal frequency, we further verified the IP3-astrocyte Ca^{2+} signals that sustain the epileptic seizure in this paper in a reliable parameter region by comparing the Ca^{2+} signal frequency of IP3-/- and IP3 non-block between the simulation and experiment cases. The results support our supposal that the Ca^{2+} signal frequency locating in a reliable region that was observed in experiments, this further suggesting the reliability of our proposed TSNA network model for describing the neuronal firing characteristics in vivo.

Virtually, all the results above in this paper have simulated the stochastic process of epileptic seizures induction under the G-protein noise. The simulation model and the results will be important refereeing knowledge for future clinical and experimental trials on the astrocytes and stochastic epilepsy. However, some points related to the dynamics epileptic seizures are still worth a trial of future studies. For example, because of the importance of GABAergic interneurons in the “shutdown” of epilepsy, the studies of GABAergic interneuron have been improved into one of the top positions in the anti-epileptic programs [67–69]. Therefore, it’s necessary to unveil the underpinning of GABAergic interneuron in inhibiting the spread of the epileptic seizure by modulating astrocytes in simulation methods. Besides, the energy consumption of epileptic seizures in human epileptic subjects was proved to be distinguishable when compared with the resting state by the combined methods of fMRI and EEG[70], therefore, unveiling the dynamical mechanism of how astrocytes transfer glucose into neuronal circumstances emerges significant for a better understanding the energy consumption theory of epileptic neuronal systems. Finally, it’s known that the febrile convulsion are generally induced with epileptic seizures by the increase of the brain temperature[71], this could be part of the factors that affects the random binding dynamics of the neuronal glutamate to the G-protein bounded receptors, thus, it’s worth to utilize the stochastic molecular dynamics simulation algorithm, e.g., Monte Carlo method, to study the stochastic mechanism of the febrile convulsion.

Appendix:

The two-compartment Pinsky–Rinzel neuron model:

The conductance-based Pinsky–Rinzel model [42] is described by the following set of ordinary differential equations:

$$C_m \frac{dV_s}{dt} = I_{Leak}^s(V_s) - I_{Na}^s(V_s, h) - I_{K-DR}(V_s, n) + \frac{g_c}{p}(V_d - V_s) \quad (14)$$

$$C_m \frac{dV_d}{dt} = I_{Leak}^d(V_d) - I_{Ca_{neuron}}(V_d, s) - I_{K-AHP}(V_d, w) - I_{K-C}(V_d, c) + \frac{g_c}{1-p}(V_s - V_d) \quad (15)$$

Where the transmembrane ion channel currents of in the soma and the dendrite can be described as the function of the corresponding potentials (V_s and V_d) and the ion channel opening variables, whose mathematical equations are shown below:

The somatic ion currents:

$$I_{Na}(V_s, h) = g_{Na} m_{\infty}^2 h (V_s - V_{Na})$$

$$I_{K-DR}(V_s, n) = g_{K-DR}n(V_s - V_K) \quad (16)$$

$$I_{Leak}^d(V_d) = g_L(V_d - V_L)$$

The dendrite ion currents:

$$\begin{aligned} I_{Ca_{neuron}}(V_d, s) &= g_{Ca_{neuron}}s^2(V_d - V_{Ca_{neuron}}) \\ I_{K-AHP}(V_d, w) &= g_{K-AHP}w(V_d - V_K) \\ I_{K-C}(V_d, c) &= g_{K-C}c\chi([Ca_{neuron}]) (V_d - V_K) \\ \chi([Ca_{neuron}]) &= \min\left(\frac{[Ca_{neuron}]}{250}, 1.0\right) \end{aligned} \quad (17)$$

In the above equations, the gating variables of h, n, s, w adapt to the biophysical models of

$$\frac{dy}{dt} = \alpha_y(x)(1-y) - \beta_y(x)y \quad (18)$$

$$x = \begin{cases} V_s & y = h, n, m \\ V_d & y = s, c \\ Ca_{neuron} & y = w \end{cases}$$

The rise rate α_y and decay rate β_y of the gating variables are obtained by the experimental adaptions in the mathematical forms of

$$\begin{aligned} \alpha_m &= \frac{0.32(13.31 - V_s)}{\exp((13.31 - V_s)/4) - 1}, \beta_m = \frac{0.28(V_s - 40.1)}{\exp((V_s - 40.1)/5) - 1} \\ \alpha_n &= \frac{0.016(35.1 - V_s)}{\exp((35.1 - V_s)/5) - 1}, \beta_n = 0.25 \exp(0.5 - 0.025V_s) \\ \alpha_h &= 0.128 \exp((17 - V_s)/18), \beta_h = \frac{4}{1 + \exp((40 - V_s)/5)} \\ \alpha_s &= \frac{1.6}{1 + \exp(-0.072(V_d - 65))}, \beta_h = \frac{0.02(V_d - 51.1)}{\exp((V_d - 51.1)/5) - 1} \\ \alpha_c &= \begin{cases} \frac{(\exp((V_d - 10)/11) - (V_d - 6.5)/27)}{2 \exp((V_d - 6.5)/27)} / 18.975 \\ \end{cases} \\ \beta_c &= \begin{cases} 2 \exp((V_d - 6.5)/27) - \alpha_c / 18.975 & V_d \leq 50 \\ 2 \exp((V_d - 6.5)/27) & V_d > 50 \end{cases} \\ \alpha_w &= \min(0.00002[Ca_{neuron}], 0.01), \beta_w = 0.001 \end{aligned}$$

Where, the $[Ca_{neuron}]$ is the calcium concentration at the dendrite and modulated by the dendrite potential, the mathematical form of $[Ca_{neuron}]$ can be described by the following equation:

$$\frac{d[Ca_{neuron}]}{dt} = -0.13g_{Ca}s^2(V_d - V_{Ca}) - 0.07[Ca_{neuron}] \quad (19)$$

The entropy theorem:

In this paper, the Shannon entropy equation was introduced to provide a way to estimate the average minimum number of bits needed to encode a string of epileptic depolarization block, DB symbols, based on the frequency of the DB symbols. As shown in the DB maps of the inserted figures in Fig. 6 in the manuscript, all the neuronal firing in one noise intensity DS case were transformed into 1-0 signals: for each non-overlapped time window of the neuronal firing, if the window voltage signal stay steady with a small noisy amplitude of 5mV, we defined the transformed signal as 1 at this time window, else, it will be 0 based on the *in vitro* epileptic depolarization block characteristics [47]. For each transformed

neuronal firing time series, the epileptic DB entropy can be described by the equation:

$$H_{DB} = -\sum_{i=1}^{N-1} p_i \log_2 p_i \quad (20)$$

Where p_i is the presence probability of a given DB symbol in each transformed series of the neuronal firing. Finally, the DB entropy in Fig. 6 was obtained by averaging all H_{DB} across all neurons in the network.

Table 1 Parameter values for the tripartite synaptic neuron-astrocyte network model and the Pinsky–Rinzel model.

Parameter	Value	Description
C_m	$3\mu\text{Fcm}^{-2}$ [42]	Membrane capacitance
g_{Na}	30mScm^{-2} [42]	Conductance of persistent sodium current
g_{K-DR}	15mScm^{-2} [42]	Conductance of potassium current
g_{k-AHP}	0.8mScm^{-2} [42]	Conductance of afterhyperpolarization potassium current
g_{K-C}	15mScm^{-2} [42]	Conductance of potassium leak current
g_{NaL}	0.05mScm^{-2} [42]	Conductance of sodium leak current
g_L	0.05mScm^{-2} [42]	Conductance of chloride leak current
g_{Ca}	10mScm^{-2} [42]	Calcium conductance
g_C	2.1mScm^{-2} [42]	Dendrite-soma process conductance
V_{Na}	115mV [42]	Reversal potential of sodium
V_K	-15mV [42]	Reversal potential of potassium
V_L	0mV [42]	Reversal potential of chloride
V_{Ca}	140mV [42]	Reversal potential of calcium
p	0.5 [39,42]	The ratio of the cell area occupied by soma and by the dendrites.
IP_3^*	$0.16\mu\text{M}$ [39,42]	The equilibrium concentration of IP3
τ_{IP_3}	7.14s [39]	The time constant of IP3
r_{IP_3}	$0.8\mu\text{M s}^{-1}$ [39]	The rate of IP3 production
c_l	0.185 [39]	The fitting parameter of the efflux calcium channel from endoplasmic reticulum (ER)
v_l	6 s^{-1} [20]	Scaling parameter of the IP3-dependet calcium channel
v_2	0.11 s^{-1} [20]	Scaling parameter of the calcium leaky channel
v_3	$0.9\mu\text{M.s}^{-1}$ [20]	Scaling parameter of the calcium pump channel
a_2	$0.2\mu\text{M.s}^{-1}$ [20]	Scaling parameter of the opening dynamics of IP3-dependet calcium channel
d_l	$0.13\mu\text{M}$ [20]	Activation parameter of the IP3-dependet calcium

		channel
d_2	$1.049 \mu\text{M}^{[39]}$	Activation parameter of the IP3-dependet calcium channel
d_3	$0.9434\mu\text{M}^{[39]}$	Inactivation parameter of the IP3-dependet calcium channel
d_5	$0.08234\mu\text{M}^{[39]}$	Activation parameter of the IP3-dependet calcium channel
ρ_{glu}	$0.785^{[20]}$	the vesicle to extra-synaptic volume fraction of the integrate synaptic glutamate
N_{glu}	$0.45^{[20]}$	Exponent constant of glutamate Hill-analysis
$g_{astro-gap}$	$2\mu\text{M s}^{-1[40]}$	The permeability rate of IP3 flow in astrocyte gap junction channels
V_T	$5\text{mV}^{[40]}$	The action potential threshold for pre-synapse releasing glutamate
κ	$2\text{s}^{[40]}$	Time constant for glutamate release process
g_{syn}	$0.045\text{mS cm}^{-2[40]}$	Conductance of AMPA synapses
E_{syn}	$140\text{mV}^{[40]}$	Reversal potential of AMPA synapses
α_s	$1\text{s}^{-1[40]}$	The increase rate of AMPA gating variable s
β_s	$0.5 \text{s}^{-1[40]}$	The decay rate of AMPA gating variable s
z	$2^{[45]}$	The valence of Ca^{2+} ion
F	$96\,489 \text{ C/mol}^{[45]}$	Faraday constant
V_{ast}	$5.233 \times 10^{13} \text{ l}^{[45]}$	The volume of an astrocyte assumed as a spherical soma
g_{astro_max}	$66\text{mM s}^{-1[44]}$	Strength of glial uptake of extracellular potassium
$\mathcal{E} k$	$1.2\text{s}^{-1[44]}$	Diffusion constant
K_{Kbath}	$4.0\text{mM}^{[44]}$	Steady state extracellular potassium concentration
K_{in}	$130\text{mM}^{[44]}$	The intercellular potassium concentration
		conductance

Acknowledgement:

This work was supported by the National Natural Science Foundation of China (Grant Nos. 12002251, 1197020421), the Natural Science Basic Research Plan in Shaanxi Province of China (Grant Nos. 2020JM-473) and the Xi'an Science and Technology Program(Grant No. 2020KJRC0055).

References:

1. R. D. Thijs, R. Surges, T. J. O'Brien, J.W. Sander. "Epilepsy in adults," *Lancet*, vol. 393, no. 10172, pp. 689-701, 2019.
2. M. C. H. Li, M. J. Cook, "Deep brain stimulation for drug-resistant epilepsy," *Epilepsia*, vol. 59, no. 2, pp. 273-290, 2018.
3. D. Friedman, J. A. French, "Clinical trials for therapeutic assessment of antiepileptic drugs in the 21st century: obstacles and solutions," *Lancet Neurol.*, vol. 11, no. 9, pp. 827-834, 2012.

4. M. K. Sidhu, J. S. Duncan, J. W. Sander, "Neuroimaging in epilepsy," *Curr. Opin. Neurol.*, vol. 31, no. 4, pp.371-378, 2018.
5. J. Daunizeau, K. E. Stephan, K. J. Friston, "Stochastic dynamic causal modelling of fMRI data: should we care about neural noise?" *Neuroimage*, vol. 62, no. 1, pp. 464-81, 2012.
6. M.O. Baud, T. Proix, V. R. Rao, et al., "Chance and risk in epilepsy," *Curr. Opin. Neurol.*, vol. 33, no. 2, pp. 163-172, 2020.
7. P. J. Karoly, D.R. Freestone, R. Boston, et al., "Interictal spikes and epileptic seizures: their relationship and underlying rhythmicity," *Brain*, vol. 139, no. Pt 4, pp. 1066-1078, 2016.
8. S. P. Burns, S. Santaniello, R. B. Yaffe, et al., "Network dynamics of the brain and influence of the epileptic seizure onset zone," *Proc. Natl. Acad. Sci. USA*, vol. 111, no. 49, pp. E5321-E5330, 2014.
9. M. A. Kramer, W. Truccolo, U. T. Eden, et al., "Human seizures self-terminate across spatial scales via a critical transition," *Proc. Natl. Acad. Sci. USA*, vol. 109, no. 51, pp. 21116-21121, 2012.
10. W. W. Lytton, A. Omurtag, "Tonic-clonic transitions in computer simulation," *J. Clin. Neurophysiol.*, vol. 24, no. 2, pp. 175-181, 2007.
11. C. Diaz Verdugo, S. Myren-Svelstad, E. Aydin, et al., "Glia-neuron interactions underlie state transitions to generalized seizures," *Nat. Commun.*, vol.10, no. 1, p. 3830, 2019.
12. D. Boison, C. Steinhäuser, "Epilepsy and astrocyte energy metabolism," *Glia*, vol. 66, no. 6, pp. 1235-1243, 2018.
13. G. Carmignoto, P. G. Haydon, "Astrocyte calcium signaling and epilepsy," *Glia*, vol. 60, no. 8, pp. 1227-1233, 2012.
14. H. R. Parri, T. M. Gould, V. Crunelli, "Spontaneous astrocytic Ca^{2+} oscillations in situ drive NMDAR-mediated neuronal excitation," *Nat. Neurosci.*, vol. 4, no. 8, pp. 803-812, 2001.
15. Araque, V. Parpura, R. P. Sanzgiri, et al., "Tripartite synapses: glia, the unacknowledged partner," *Trends Neurosci.*, vol. 22, no. 5, pp. 208-215, 1999.
16. Witthoft, J. A. Filosa, G. E. Karniadakis, "Potassium buffering in the neurovascular unit: models and sensitivity analysis," *Biophys. J.*, vol. 105, no. 9, pp. 2046-2054, 2013.
17. G. Ullah, S. J. Schiff, "Assimilating seizure dynamics," *PLoS Comput. Biol.*, vol. 6, no. 5, p. e1000776, 2010.
18. M. Du, J. Li, L. Chen, et al., "Astrocytic Kir4.1 channels and gap junctions account for spontaneous epileptic seizure," *PLoS Comput. Biol.*, vol. 14, no. 3, p. e1005877, 2018.
19. S. Nadkarni, P. Jung, "Spontaneous oscillations of dressed neurons: a new mechanism for epilepsy?" *Phys. Rev. Lett.*, vol. 91, no. 26, p. 268101, 2003.
20. S. Nadkarni, P. Jung, "Dressed neurons: modeling neural–glial interactions," *Phys. Biol.*, vol. 1, no. 1, p. 35, 2004.
21. J. J. Li, J. Tang, J. Ma, et al., "Dynamic transition of neuronal firing induced by abnormal astrocytic glutamate oscillation" *Sci. Rep.*, vol. 6, p. 10, 2016.
22. J. A. Hubbard, J. I. Szu, J. M. Yonan, et al., "Regulation of astrocyte glutamate transporter-1 (GLT1) and aquaporin-4 (AQP4) expression in a model of epilepsy," *Exp. Neurol.*, vol. 283, pp. 85-96, 2016.
23. A. Durkee, A. Covelo, Lines J, et al., "G(i/o) protein-coupled receptors inhibit neurons but activate astrocytes and stimulate gliotransmission," *Glia*, vol. 67, no. 6, pp. 1076-1093, 2019.

24. A. Durkee, A. Araque, "Diversity and specificity of astrocyte–neuron communication," *Neuroscience*, vol. 396, pp. 73-78, 2019.
25. Cavaccini, C. Durkee, P. Kofuji, R. Tonini, A. Araque, "Astrocyte signaling gates long-term depression at corticostriatal synapses of the direct pathway," *J. Neurosci.*, vol. 40, no. 30, pp. 5757-5768, 2020.
26. P.C. Bressloff, "Mean-field theory of globally coupled integrate-and-fire neural oscillators with dynamic synapses," *Phys. Rev. E.*, vol. 60 no. 2PtB, pp. 2160-2170, 1999.
27. R. Chaudhuri, K. Knoblauch, M.A. Gariel, et al., "A large-scale circuit mechanism for hierarchical dynamical processing in the primate cortex," *Neuron*, vol. 88, no. 2, pp. 419-431, 2015.
28. M.R. Joglekar, J.F. Mejias, G.R. Yang, et al., "Inter-areal balanced amplification enhances signal propagation in a large-scale circuit model of the primate cortex," *Neuron*, vol. 98, no. 1, pp. 222-234, 2018.
29. Liu, C. Zhou, J. Wang, et al., "Delayed feedback-based suppression of pathological oscillations in a neural mass model," *IEEE Trans Cybern*, Jul. 2019. doi: 10.1109/TCYB.2019.2923317.
30. P. N. Taylor, Y. Wang, M. Goodfellow, et al., "A computational study of stimulus driven epileptic seizure abatement," *PLoS One*, vol. 9, no. 12, p. 26, 2014.
31. M. Chen, D. Guo, T. Wang, et al., "Bidirectional control of absence seizures by the basal ganglia: a computational evidence," *PLoS Comput. Biol.*, vol. 10, no. 3, p. e1003495, 2014.
32. Fan, S. Liu, Q. Wang, "Stimulus-induced epileptic spike-wave discharges in thalamocortical model with disinhibition," *Sci. Rep.*, vol. 6, p. 37703, 2016.
33. P. R. Bauer, R. D. Thijs, R. J. Lamberts, et al., "Dynamics of convulsive seizure termination and postictal generalized EEG suppression," *Brain*, vol. 140, no. 3, pp. 655-668, 2017.
34. H. Zhang, P. Xiao, "Seizure dynamics of coupled oscillators with epileptor field model," *Int. J. Bifurcat. Chaos*, vol. 28, no.03, p. 1850041, 2018.
35. C. Giaume, A. Koulakoff, L. Roux, et al., "Astroglial networks: a step further in neuroglial and gliovascular interactions," *Nat. Rev. Neurosci.*, vol. 11, no. 2, pp. 87-99, 2010.
36. B.S. Khakh, B. Deneen, "The emerging nature of astrocyte diversity," *Annu. Rev. Neurosci.*, vol. 42, no. 187-207, 2019.
37. S. Nadkarni, Jung P, Levine H. "Astrocytes optimize the synaptic transmission of information," *PLoS Comput. Biol.*, vol. 4, no. 5, p. e1000088, 2008.
38. C. Stringer, M. Pachitariu, N. Steinmetz, et al., "High-dimensional geometry of population responses in visual cortex," *Nature*, vol. 571 no. 7765, pp. 361-365, 2019.
39. Y. X. Li, J. Rinzel, "Equations for InsP3 receptor-mediated $[Ca^{2+}]_i$ oscillations derived from a detailed kinetic model: a Hodgkin-Huxley like formalism," *J. Theor. Biol.*, vol. 166, no. 4, pp. 461-473, 1994.
40. M. Goldberg, M. De Pittà, V. Volman, et al., "Nonlinear gap junctions enable long-distance propagation of pulsating calcium waves in astrocyte networks," *PLoS Comput. Biol.*, vol. 6, no. 8, p. e1000909, 2010.
41. Destexhe, Z. F. Mainen, T. J. Sejnowski, "Synthesis of models for excitable membranes, synaptic transmission and neuromodulation using a common kinetic formalism," *J. Comput. Neurosci.*, vol. 1, no. 3, pp. 195-230, 1994.
42. P. F. Pinsky, J. Rinzel, "Intrinsic and network rhythmogenesis in a reduced Traub model for CA3 neurons," *J. Comput. Neurosci.*, vol. 1 no. 1-2, pp. 39-60, 1994.

43. N. Brunel, X. J. Wang, "What determines the frequency of fast network oscillations with irregular neural discharges? I. Synaptic dynamics and excitation-inhibition balance," *J. Neurophysiol.*, vol. 90, no. 1, pp. 415-430, 2003.
44. Fröhlich, T. J. Sejnowski, M. Bazhenov, "Network bistability mediates spontaneous transitions between normal and pathological brain states," *J. Neurosci.*, vol. 30, no. 32, pp. 10734-10743, 2010.
45. S. Zeng, B. Li, S. Zeng, et al., "Simulation of spontaneous Ca^{2+} oscillations in astrocytes mediated by voltage-gated calcium channels," *Biophys. J.*, vol. 97, no. 9, pp. 2429-2437, 2009.
46. J. Li, S. I. Kronemer, W. X. Herman, H. Kwon, J. H. Ryu, C. Micek, Y. Wu, J. Gerrard, D. D. Spencer, H. Blumenfeld, "Default mode and visual network activity in an attention task: Direct measurement with intracranial EEG," *NeuroImage*, vol. 201, p. 116003, 2019.
47. J. Ziburkus, J. R. Cressman, E. Barreto, S. J. Schiff, "Interneuron and pyramidal cell interplay during in vitro seizure-like events," *J. Neurophysiol.*, vol. 95, no. 6, pp. 3948-3954, 2006.
48. M. Dümpelmann, J. Jacobs, K. Kerber, et al., "Automatic 80-250Hz "ripple" high frequency oscillation detection in invasive subdural grid and strip recordings in epilepsy by a radial basis function neural network," *Clin. Neurophysiol.*, vol. 123, no. 9, pp. 1721-1731, 2012.
49. L. Fairhall, G. D. Lewen, W. Bialek, et al., "Efficiency and ambiguity in an adaptive neural code," *Nature*, vol. 412, no. 6849, pp. 787-792, 2001.
50. W. B. Levy, R. A. Baxter, "Energy-efficient neuronal computation via quantal synaptic failures," *J. Neurosci.*, vol. 22, no. 11, pp. 4746-4755, 2002.
51. S. S. Poil, R. H. Arstone, H. D. Mansvelder, et al., "Critical-state dynamics of avalanches and oscillations jointly emerge from balanced excitation/inhibition in neuronal networks," *J. Neurosci.*, vol. 32, no. 29, pp. 9817-9823, 2012.
52. Wang, J. Ma, Y. Chen, et al., "Effect of an autapse on the firing pattern transition in a bursting neuron," *Commun. Nonlinear Sci. Numer. Simul.*, vol. 19, no. 9, pp. 3242-3254, 2014.
53. D. Dorval, G. S. Russo, T. Hashimoto, et al., "Deep brain stimulation reduces neuronal entropy in the MPTP-primate model of Parkinson's disease," *J. Neurophysiol.*, vol. 100, no. 5, pp. 2807-2818, 2008.
54. N. K. Codadu, R. T. Graham, R. J. Burman, et al., "Divergent paths to seizure-like events," *Physiol. Rep.*, vol. 7, no. 19, p. e14226, 2019.
55. M. Wang, Y. He, T. J. Sejnowski, et al., "Brain-state dependent astrocytic Ca^{2+} signals are coupled to both positive and negative BOLD-fMRI signals," *Proc Natl Acad Sci U S A*, vol. 115, no. 7, pp. E1647-E1656, 2018.
56. X. Gu, W. Chen, N. D. Volkow, et al., "Synchronized astrocytic Ca^{2+} responses in neurovascular coupling during somatosensory stimulation and for the resting state," *Cell Rep.*, vol. 23, no. 13, pp. 3878-3890, 2018.
57. R. Srinivasan, B. S. Huang, S. Venugopal, et al., " Ca^{2+} signaling in astrocytes from $\text{Ip3r2}^{-/-}$ mice in brain slices and during startle responses in vivo," *Nat. Neurosci.*, vol. 18, no. 5, pp. 708-717, 2015.
58. M. Gómez-Gonzalo, G. Losi, A. Chiavegato, et al., "An excitatory loop with astrocytes contributes to drive neurons to seizure threshold," *PLoS Biol.*, vol. 8, no. 4, p. e1000352, 2010.
59. C. Álvarez-Ferradas, J. C. Morales, M. Wellmann, et al., "Enhanced astroglial Ca^{2+} signaling increases excitatory synaptic strength in the epileptic brain," *Glia*, 2015.

60. J. C. Fordsmann, R. P. Murmu, C. Cai, et al., "Spontaneous astrocytic Ca(2+) activity abounds in electrically suppressed ischemic penumbra of aged mice," *Glia*, vol. 67, no. 1, pp. 37-52, 2019.
61. K. Kanemaru, H. Sekiya, M. Xu, et al., "In vivo visualization of subtle, transient, and local activity of astrocytes using an ultrasensitive Ca(2+) indicator", *Cell Rep.*, vol. 8, no. 1, pp. 311-318, 2014.
62. Volterra, N. Liaudet, I. Savtchouk, "Astrocyte Ca²⁺ signalling: an unexpected complexity," *Nat. Rev. Neurosci.*, vol. 15, no. 5, pp. 327-335, 2014.
63. Panatier et al., "Astrocytes are endogenous regulators of basal transmission at central synapses," *Cell*, vol. 146, no. 785-798, 2011.
64. S. Boie, J. Chen, M. J. Sanderson, et al., "The relative contributions of store-operated and voltage-gated Ca(2+) channels to the control of Ca(2+) oscillations in airway smooth muscle," *J. Physiol.*, vol. 595, no. 10, pp. 3129-3141, 2017.
65. J. Chen, M. J. Sanderson, "Store-operated calcium entry is required for sustained contraction and Ca(2+) oscillations of airway smooth muscle," *J. Physiol.*, vol. 595, no. 10, pp. 3203-3218, 2017.
66. P. Janz, N. Schwaderlapp, K. Heining, et al., "Early tissue damage and microstructural reorganization predict disease severity in experimental epilepsy," *Elife*, vol. 6, p. e25742, 2017.
67. P. Winkler, H. J. Luhmann, W. Kilb, "Taurine potentiates the anticonvulsive effect of the GABA(A) agonist muscimol and pentobarbital in the immature mouse hippocampus," *Epilepsia*, vol. 60 no. 3, pp. 464-474, 2019.
68. R. L. Macdonald, "GABAA receptor defects can cause epilepsy," *Epilepsy Curr.*, vol. 1, no. 2, p. 74, 2001.
69. T. P. Ladas, C. C. Chiang, L. E. Gonzalez-Reyes, et al., "Seizure reduction through interneuron-mediated entrainment using low frequency optical stimulation," *Exp. Neurol.*, vol. 269, pp. 120-132, 2015.
70. J. N. Guo, R. Kim, Y. Chen, et al., "Impaired consciousness in patients with absence seizures investigated by functional MRI, EEG, and behavioural measures: a cross-sectional study," *Lancet Neurol.*, vol. 15, no. 13, pp. 1336-1345, 2016.
71. R. C. Scott, M. D. King, D. G. Gadian, B. G. Neville, A. Connelly, "Hippocampal abnormalities after prolonged febrile convulsion: a longitudinal MRI study," *Brain*, vol. 126, no. Pt11, pp. 2551-2557, 2003.